Nanoscale

Cite this: *Nanoscale*, 2012, **4**, 6876

www.rsc.org/nanoscale

PAPER

Sm@C_{2v}(3)-C_{80}: site-hopping motion of endohedral Sm atom and metal-induced effect on redox profile†

Wei Xu,[b] Ben Niu,[bc] Zujin Shi,*[b] Yongfu Lian*[c] and Lai Feng*[a]

Received 8th August 2012, Accepted 4th September 2012
DOI: 10.1039/c2nr32193a

A new metallofullerene Sm@C_{2v}(3)-C_{80} was synthesized and characterized. X-Ray analysis showed that the endohedral Sm atom undergoes a hopping motion between several off-center sites, even at low temperature. In addition, a comparative electrochemical study between Sm@C_{2v}(3)-C_{80} and Yb@C_{2v}(3)-C_{80} revealed their different redox potentials, suggesting a metal-induced effect on their redox profiles.

Introduction

Fullerene species doped with metals or metallic clusters inside the cage cavities have emerged as a novel class of carbon–metal hybrids and are referred to as endohedral metallofullerenes (EMFs). It has been shown that a variety of metals including most of the Group I–IV elements can be trapped inside a fullerene cage in multiple forms.[1–4] In recent years, many studies have focused on understanding their structural features as well as their electrochemical, chemical and physical properties, which might vary depending on the nature of endohedral metallic species.[5–15]

In particular, fullerenes containing one metal atom (*i.e.*, M@C_{2n}) are considered as the simplest model species of EMFs. It has been proved that the endohedral metal exhibits an oxidation state and donates a number of electrons to the fullerene cage. Thus, an important structural feature of M@C_{2n} regards the location or motional behavior of endohedral metal, which actually reflects the interplay between the metal ion and fullerene cage. To date, many efforts have been made to reveal such feature. Summarizing previous studies, it has been shown that the endohedral metal such as La, Ce, Gd or Y, which usually exhibits a 3+ oxidation state, is highly localized inside a middle-sized cage of C_{2v}-C_{82}.[16–18] Besides, a motional Sm atom that adopts a 2+ oxidation state was identified inside larger cages such as C_{84} and C_{90}–C_{94}.[19–21] It appears that the cage size plays an important role in guiding the behavior of the endohedral metal. However, it is still unclear whether different metal ions have similar locations or motional behaviors inside a closed and nanometer-sized fullerene cage.

C_{2v}(3)-C_{80} is another middle-sized cage, which has been never found in empty fullerenes but is common for EMFs.[22–24] Specifically, La@C_{2v}(3)-C_{80}–$C_6H_3Cl_2$ (ref. 22) and Yb@C_{2v}(3)-C_{80} (ref. 23 and 24) are two well-studied species with a C_{2v}(3)-C_{80} cage. In both cases, the endohedral metals La and Yb, which are either trivalent or divalent, are highly localized at a specific site. It has been proposed that such metal location either corresponds to the electrostatic potential minimum inside $[C_{2v}(3)\text{-}C_{80}\text{–}C_6H_3Cl_2]^{3-}$ or affords largest coordination interaction between metal and cage. However, because of the lack of additional evidence, it is so far unknown how the cage of C_{2v}(3)-C_{80} interplays with other metals.

Herein, we report a new metallofullerene Sm@C_{2v}(3)-C_{80}, including its preparation, structural characterizations and electrochemical studies. Although this metallofullerene possesses the same cage of C_{2v}(3)-C_{80}, it is shown that the endohedral Sm atom displays a site-hopping motion rather than being highly localized at a specific site. In addition, the redox properties of Sm@C_{2v}(3)-C_{80} are compared with those of Yb@C_{2v}(3)-C_{80}, showing a metal-induced effect on redox profile.

Experimental

Synthesis and isolation

The synthesis of Sm–metallofullerenes was described in earlier studies.[25] Briefly, the carbon soot containing Sm–metallofullerenes were synthesized by a DC arc discharge method in a He atmosphere at 720 Torr using a composite rod made of graphite and $SmNi_2$ alloy. The soot was collected, extracted and then separated by multi-stage high performance liquid chromatography (HPLC, LC908-C60, Japan Analytical Industry Co.) using toluene as eluent. A 5PYE column (ø20 × 250 mm, Nacalai Co., Japan), a Buckyprep column (ø20 × 250 mm, Nacalai Co., Japan) and a Buckyprep-M column (ø20 × 250 mm, Nacalai Co., Japan) were employed for separation.

[a]*Jiangsu Key Laboratory of Thin Films and School of Energy, Soochow University, Suzhou 215006, P. R. China. E-mail: fenglai@suda.edu.cn*
[b]*Beijing National Laboratory for Molecular Sciences, State Key Lab of Rare Earth Materials Chemistry and Applications, College of Chemistry and Molecular Engineering, Peking University, Beijing 100871, P. R. China. E-mail: zjshi@pku.edu.cn*
[c]*School of Chemistry and Materials Science, Heilongjiang University, Harbin 150080, P. R. China. E-mail: chyflian@hlju.edu.cn*
† CCDC reference number 894168. For crystallographic data in CIF or other electronic format see DOI: 10.1039/c2nr32193a

Spectroscopy

^{13}C NMR spectra were recorded on an Avance-500 spectrometer (Bruker Analytik, Germany) with a CryoProbe system, using a capillary tube of acetone-d_6 as external lock and CS_2 as solvent. Absorption spectra were recorded in a CS_2 solution with a Shimadzu UV-3150 spectrometer using a quartz cell and 1 nm resolution. Matrix-assisted laser desorption-ionization time-of-flight (MALDI-TOF) mass spectrum was recorded with a Bruker BIFLEX-III mass spectrometer. The measurements were performed in both positive and negative ion modes.

Single-crystal X-ray diffraction analysis

Black co-crystals of Sm@C_{2v}(3)-C_{80}/Ni^{II}(OEP) were obtained by allowing the benzene solution of fullerene and the chloroform solution of Ni^{II}(OEP) to diffuse together. X-Ray data were collected at 90 K using a diffractometer (APEX II; Bruker Analytik GmbH) equipped with a CCD collector.† The multi-scan method was used for absorption correction. The structure was resolved using direct methods (SHELXS97) and refined on F^2 using full-matrix least squares with SHELXL97.[26] In refinement, the intact cage was modeled *via* the crystallographic mirror plane. Hydrogen atoms were added geometrically and refined with a riding model.

Electrochemistry

Differential pulse voltammetry (DPV) and cyclic voltammetry (CV) were carried out in *o*-dihlorobenzene (*o*-DCB) using a BAS CW-50 instrument. A conventional three-electrode cell consisting of a platinum working electrode, a platinum counter-electrode, and a saturated calomel reference electrode (SCE) was used for both measurements. 0.05 M $(n\text{-}Bu)_4NPF_6$ was used as the supporting electrolyte. All potentials were recorded against a SCE reference electrode and corrected against Fc/Fc^+. DPV and CV were measured at a scan rate of 20 and 50 mV s^{-1}, respectively.

Results and discussion

The purity of the Sm@C_{2v}(3)-C_{80} sample was checked by HPLC and the composition of SmC_{80} was confirmed by MALDI-TOF mass analysis (see Fig. 1). The absolute structure of Sm@C_{2v}(3)-C_{80} was determined *via* a single-crystal X-ray diffraction (XRD) study.† Cocrystals of Sm@C_{2v}(3)-C_{80}/[Ni^{II}(OEP)] suitable for X-ray analysis were obtained by slow diffusion of a benzene solution of EMF into a $CHCl_3$ solution of [Ni^{II}(OEP)]. The molecular structure was resolved and refined in a *C*2/*m* space group.[27] Fig. 2 shows the X-ray structure of Sm@C_{2v}(3)-C_{80} together with an adjacent [Ni^{II}(OEP)] moiety. In fact, two orientations of the C_{2v}(3)-C_{80} cage with fractional occupancies of 0.289 and 0.221 are clearly identified. Nevertheless, the C_2 axes of these disordered cages are similarly aligned relative to the porphyrin plane. Generally, the porphyrin moiety tends to approach the flat region of C_{2v}(3)-C_{80} cage with the shortest nickel-to-cage carbon distance ranging from 2.812 to 2.837 Å. It appears that in this way the largest π–π stacking between fullerene and porphyrin moieties can be achieved.

Inside the C_{2v}(3)-C_{80} cage, there are seven Sm-sites with fractional occupancies ranging from 0.224 for Sm1 to 0.005 for Sm7. As shown in Fig. 3a, all these Sm-sites, including those generated *via* the crystallographic mirror plane, are located off-center. Among them, the ratio of Sm1 to Sm2 sites is close to that between two cage orientations. It is likely that each Sm-site corresponds to either cage orientation. Besides, there are five additional Sm-sites inside the cage, among which Sm4 and Sm6 sites are nearly located in the opposite side of the cage, indicating the hopping motion of the encapsulated Sm atom between these sites even at 90 K. In contrast, inside the same cage, Yb atom is highly localized below 173 K, as previously suggested. Accordingly, somewhat different metal–cage interactions might be proposed for Sm@C_{2v}(3)-C_{80} and Yb@C_{2v}(3)-C_{80}, even though these endohedral metals exhibit the same oxidation state of 2+. Moreover, the Sm1–cage relationship is depicted in Fig. 3b. Nevertheless, because the cage is bisected by the crystallographic mirror plane, further assignment of Sm1 or Sm1A relative to the depicted cage orientation is impossible. Particularly, Sm1 is situated under a pentagonal ring with a centroid-to-metal distance of 2.239 Å, while Sm1A is under a hexagonal ring with a similar distance of 2.342 Å, suggesting either an η^5 or an η^6 metal–cage contact for Sm@C_{2v}(3)-C_{80}.

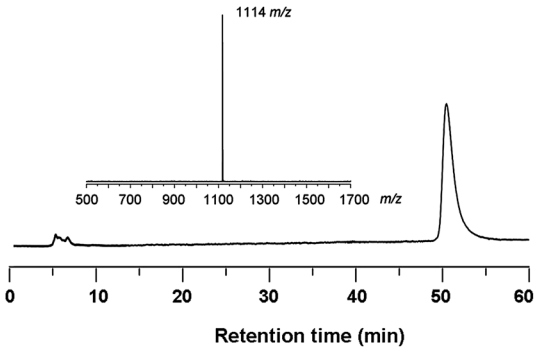

Fig. 1 HPLC profile of the isolated Sm@C_{2v}(3)-C_{80} on Buckyprep column using toluene as eluent (flow rate: 12 mL min^{-1}; detection wavelength: 330 nm). The inset shows the positive-ion MALDI-TOF mass spectrum.

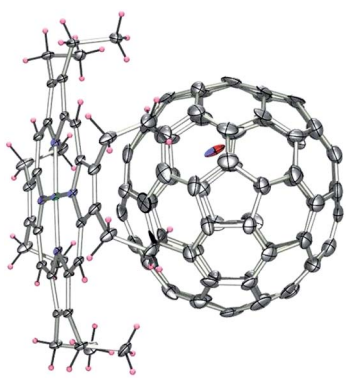

Fig. 2 ORTEP drawing of Sm@C_{2v}(3)-C_{80}·Ni^{II}(OEP) with 30% thermal ellipsoids, showing the intermolecular interaction. The major Sm site with a fractional occupancy of 0.223 and the major cage position with a fractional occupancy of 0.289 are depicted. The solvent molecules are omitted for clarity.

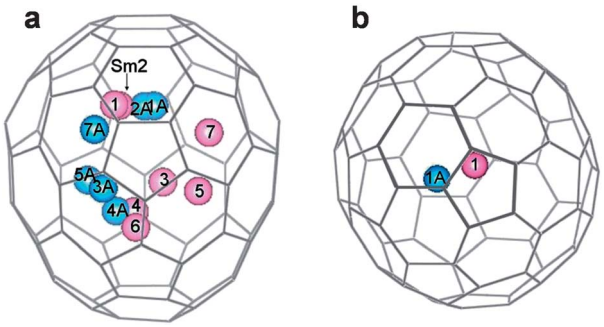

Fig. 3 Perspective views of Sm@C_{2v}(3)-C_{80}, showing the various partially occupied Sm sites inside the major cage (a) and the Sm1–cage relationship (b). Those Sm sites labeled "A" are generated *via* the crystallographic mirror plane. Fractional occupancies of Sm sites are following: Sm1, 0.223(12); Sm2, 0.190(12); Sm3, 0.0159(10); Sm4, 0.0176(9); Sm5, 0.0089(9); Sm6, 0.0185(18); Sm7, 0.0047(8).

Furthermore, Sm@C_{2v}(3)-C_{80} was characterized by ^{13}C NMR. As shown in Fig. 4, the ^{13}C NMR spectrum displays 17 signals with full intensity and another six signals with half intensity in the range 190–110 ppm at 293 K.[28] These results corroborate well with the C_{2v}-symmetric C_{80} cage[29] and are fully consistent with the XRD result. Note that the ^{13}C signals of Yb@C_{2v}(3)-C_{80} were observed in the range 155–127 ppm.[23] Thus, the ^{13}C signal distribution of Sm@C_{2v}(3)-C_{80} is much wider than that of Yb@C_{2v}(3)-C_{80}. The six unpaired f-electrons on the endohedral Sm atom might account for the greatly shifted ^{13}C signals, which significantly affect the local magnetic field and the fast relaxation of ^{13}C nuclear spins on the nearby cage carbons. In addition, the UV-Vis-NIR spectrum of Sm@C_{2v}(3)-C_{80} was recorded in a CS_2 solution, as shown in Fig. 5. All the featured absorptions observed at 1100, 855, 705, 586 and 483 nm are very close to those of Yb@C_{2v}(3)-C_{80}.[23] Besides, the spectral onset positions of these two analogues are both identified at around 1500 nm, suggesting their similar electronic structures.

To further probe the electronic structural feature of Sm@C_{2v}(3)-C_{80}, its electrochemical properties were investigated by means of cyclic voltammetry (CV) and differential pulse voltammetry (DPV). As shown in Fig. 6, the DPV profile suggests four one-electron reductive steps in the cathodic side and two one-electron oxidative steps in the anodic side. All the redox potentials obtained from CV and DPV are summarized in Table 1.

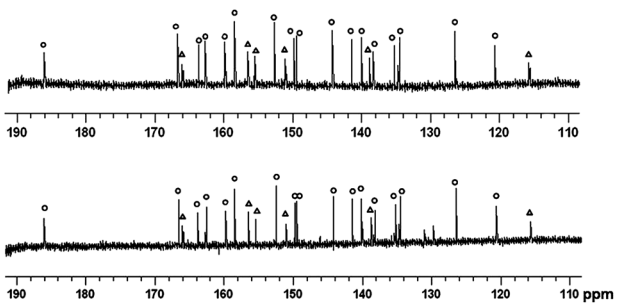

Fig. 4 ^{13}C NMR spectra (125 MHz, in CS_2 using acetone-d_6 as internal lock, 293 K) of Sm@C_{2v}(3)-C_{80} in proton-coupled (up) and proton-decoupled modes (down). ○ and Δ indicate the signals with full intensity and half intensity, respectively.

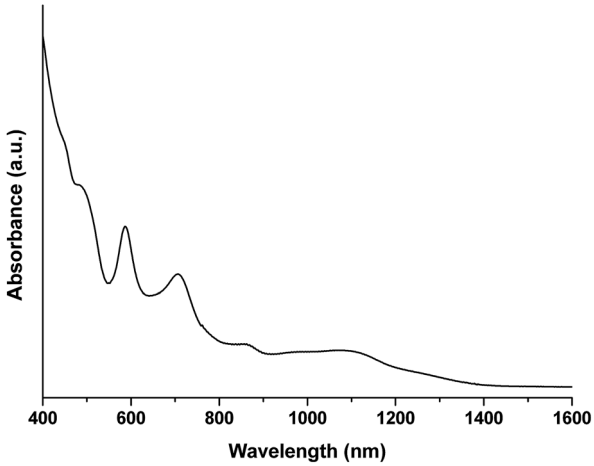

Fig. 5 UV-vis-NIR absorption spectrum of Sm@C_{2v}(3)-C_{80} in a CS_2 solution.

Compared with Yb@C_{2v}(3)-C_{80}, it is easier for Sm@C_{2v}(3)-C_{80} to be reduced (by 40 mV) and more difficult for it to be oxidized (by 90 mV). Consequently, the electrochemical potential gap of Sm@C_{2v}(3)-C_{80} is 1.28 V that is 50 mV wider than that of

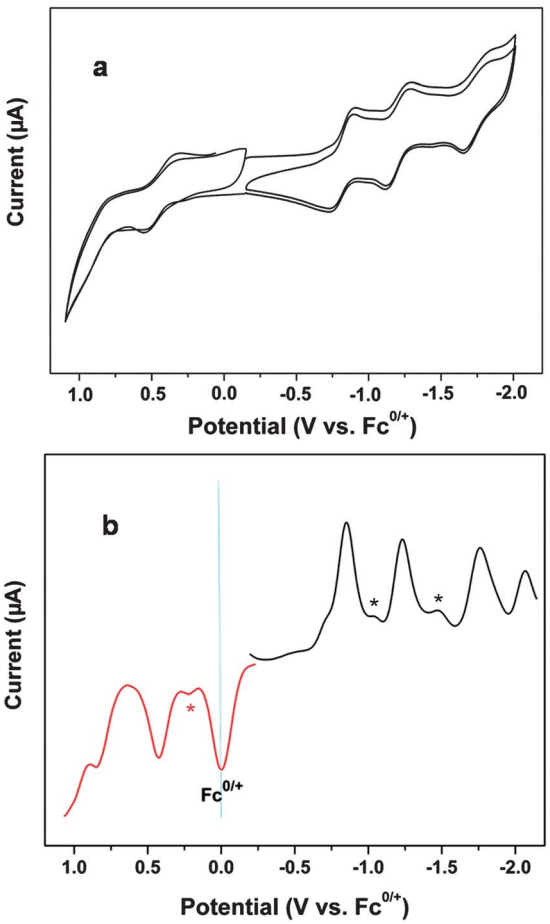

Fig. 6 Cyclic voltammograms (a) and differential pulse voltammogram (b) of Sm@C_{2v}(3)-C_{80} in *o*-dichlorobenzene (0.05 M (*n*-Bu)$_4$NPF$_6$, scan rate: 100 mV s^{-1} and 20 mV s^{-1} for CV and DPV, respectively). * corresponds to the trace impurities in either sample or solvent.

Table 1 Redox potentials (V *vs.* $Fc^{0/+}$)[a] of Sm@C_{2v}(3)-C_{80} and Yb@C_{2v}(3)-C_{80}

	$^{ox}E_2$	$^{ox}E_1$	$^{red}E_1$	$^{red}E_2$	$^{red}E_3$	$^{red}E_4$	$^{ox}E_1 - {}^{red}E_1$
Sm@C_{2v}(3)-C_{80}	0.85[b]	0.43[c]	−0.85[c]	−1.23[c]	−1.76[c]	−2.07[b]	1.28
Yb@C_{2v}(3)-C_{80}[d]	0.78	0.34	−0.89	−1.27	−1.87	−2.13	1.23

[a] Half-cell potentials unless otherwise noted. [b] DPV value. [c] Reversible process confirmed by CV. [d] Ref. 23.

Yb@C_{2v}(3)-C_{80}. Such a potential difference might suggest a significant correlation between the endohedral divalent metal and the redox properties of M@C_{2v}(3)-C_{80}. A similar trend is also detectable elsewhere: Previous studies have reported an easier one-electron reduction of Sm@C_{2v}-C_{82} ($^{red}E_{1/2} = -0.28$ V)[25] relative to that of Yb@C_{2v}-C_{82} ($^{red}E_{1/2} = -0.33$ V).[23,30] However, trivalent EMFs such as the well studied M@C_{2v}-C_{82} present a reverse and less remarkable trend.[5] For instance, compared to Gd@C_{2v}-C_{82}, La@C_{2v}-C_{82}, which contains a larger metal cation, they undergo an easier one-electron oxidation and more-difficult one-electron reduction.[31] Their redox potentials differ by only 20–30 mV. To this end, we can conclude that there is a metal-induced effect on the redox properties of M@C_{2v}(3)-C_{80} (M = divalent metal), which is otherwise less remarkable for the well-studied M@C_{2v}-C_{82} (M = trivalent metal). Nevertheless, most redox processes of Sm@C_{2v}(3)-C_{80} are fully reversible, as revealed by CV measurements. Such performance is similar to that of Yb@C_{2v}(3)-C_{80}.

Conclusions

In conclusion, we have prepared and characterized a new metallofullerene Sm@C_{2v}(3)-C_{80} by means of mass, UV-Vis-NIR, NMR spectroscopies and XRD studies. Specifically, XRD analysis showed that the endohedral Sm atom undergoes a hopping motion between several off-center sites even at low temperature. In addition, a comparative electrochemical study between Sm@C_{2v}(3)-C_{80} and Yb@C_{2v}(3)-C_{80} revealed their different redox potentials, suggesting a metal-induced effect on the redox profiles of these metallofullerenes.

Acknowledgements

This work is supported in part by NNSF of China (no. 21171013), the Ministry of Science and Technology of China (no. 2013CB933402), and the NSF of Jiangsu province of China (no. BK2012611). Also, we are grateful to Prof. T. Akasaka and Dr M. Suzuki at University of Tsukuba for their helpful discussions and XRD measurements.

Notes and references

1 T. Akasaka and S. Nagase, *Endofullerenes: a New Family of Carbon Clusters*, Kluwer, Dordrecht, 2002.
2 L. Dunsch and S. Yang, *Small*, 2007, **3**, 1298.
3 L. Feng, T. Akasaka and S. Nagase, in *Carbon Nanotubes and Related Structures*, ed. D. M. Guldi and N. Martin, Wiley-VCH, Weinheim, 2010, p. 455.
4 X. Lu, T. Akasaka and S. Nagase, *Chem. Commun.*, 2011, **47**, 5942.
5 M. N. Chaur, F. Melin, A. L. Ortiz and L. Echegoyen, *Angew. Chem., Int. Ed.*, 2009, **48**, 7514.
6 Y. Iiduka, O. Ikenaga, A. Sakuraba, T. Wakahara, T. Tsuchiya, Y. Maeda, T. Nakahodo, T. Akasaka, M. Kako, N. Mizorogi and S. Nagase, *J. Am. Chem. Soc.*, 2005, **127**, 9956.
7 L. Feng, T. Wakahara, T. Nakahodo, T. Tsuchiya, Q. Piao, Y. Maeda, Y. Lian, T. Akasaka, E. Horn, K. Yoza, T. Kato, N. Mizorogi and S. Nagase, *Chem.–Eur. J.*, 2006, **12**, 5578.
8 L. Feng, S. G. Radhakrishnan, N. Mizorogi, Z. Slanina, H. Nikawa, T. Tsuchiya, T. Akasaka, S. Nagase, N. Martín and D. M. Guldi, *J. Am. Chem. Soc.*, 2011, **133**, 7608.
9 A. Rodríguez-Fortea, A. L. Balch and J. M. Poblet, *Chem. Soc. Rev.*, 2011, **40**, 3551.
10 S. Yang, F. Liu, C. Chen, M. Jiao and T. Wei, *Chem. Commun.*, 2011, **47**, 11822.
11 L. Feng, M. Rudolf, S. Wolfrum, A. Troeger, Z. Slanina, T. Akasaka, S. Nagase, N. Martin, T. Ameri, C. J. Brabec and D. M. Guldi, *J. Am. Chem. Soc.*, 2012, **134**, 12190.
12 S. Sato, S. Seki, G. Luo, M. Suzuki, J. Lu, S. Nagase and T. Akasaka, *J. Am. Chem. Soc.*, 2012, **134**, 11681.
13 Y. Ma, T. Wang, J. Wu, Y. Feng, W. Xu, L. Jiang, J. Zheng, C. Shu and C. Wang, *Nanoscale*, 2011, **3**, 4955.
14 S. S. Babu, H. Mohwald and T. Nakanishi, *Chem. Soc. Rev.*, 2010, **39**, 4021.
15 S. Kobayashi, S. Mori, S. Iida, H. Ando, T. Takenobu, Y. Taguchi, A. Fujiwara, A. Taninaka, H. Shinohara and Y. Iwasa, *J. Am. Chem. Soc.*, 2003, **125**, 8116.
16 Y. Maeda, T. Tsuchiya, X. Lu, Y. Takano, T. Akasaka and S. Nagase, *Nanoscale*, 2011, **3**, 2421.
17 M. Yamada, T. Akasaka and S. Nagase, *Acc. Chem. Res.*, 2010, **43**, 92.
18 K. Kobayashi and S. Nagase, *Chem. Phys. Lett.*, 1998, **282**, 325.
19 H. Yang, M. Yu, H. Jin, Z. Liu, M. Yao, B. Liu, M. M. Olmstead and A. L. Balch, *J. Am. Chem. Soc.*, 2012, **134**, 5331.
20 H. Jin, H. Yang, M. Yu, Z. Liu, C. M. Beavers, M. M. Olmstead and A. L. Balch, *J. Am. Chem. Soc.*, 2012, **134**, 10933.
21 H. Yang, H. Jin, H. Zhen, Z. Wang, Z. Liu, C. M. Beavers, B. Q. Mercado, M. M. Olmstead and A. L. Balch, *J. Am. Chem. Soc.*, 2011, **133**, 6299.
22 H. Nikawa, T. Yamada, B. P. Cao, N. Mizorogi, Z. Slanina, T. Tsuchiya, T. Akasaka, K. Yoza and S. Nagase, *J. Am. Chem. Soc.*, 2009, **131**, 10950.
23 X. Lu, Z. Slanina, T. Akasaka, T. Tsuchiya, N. Mizorogi and S. Nagase, *J. Am. Chem. Soc.*, 2010, **132**, 5896.
24 X. Lu, Y. Lian, C. M. Beavers, N. Mizorogi, Z. Slanina, S. Nagase and T. Akasaka, *J. Am. Chem. Soc.*, 2011, **133**, 10772.
25 J. Liu, Z. Shi and Z. Gu, *Chem.–Asian J.*, 2009, **4**, 1703.
26 G. M. Sheldrick, *Acta Crystallogr., Sect. A: Found. Crystallogr.*, 2007, **64**, 112.
27 Crystal data for Sm@C_{2v}(3)-C_{80}·Ni^{II}(OEP)·1.79C_6H_6·0.21$CHCl_3$: $C_{126.95}H_{54.95}C_{l0.63}SmN_4Ni$, Mr = 1867.49, 0.25 × 0.19 × 0.15 mm, monoclinic, *C2/m*, *a* = 25.254(3), *b* = 14.979(18), *c* = 19.724(2), β = 94.323(1)o, *V*= 7440.0 Å^3, *Z* = 4, ρ_{calc} = 1.667 g cm^{-3}, μ(MoKa) =1.127 mm^{-1}, θ =4.30–27.87o, *T* = 90 K, R_1 = 0.0899, wR_2 = 0.1933 for all data; R_1 = 0.0706, wR_2 = 0.1773 for 9171 reflections ($I > 2.0\sigma(I)$) with 1215 parameters. Maximum residual electron density 1.378 e Å^{-3}. CCDC 894168.
28 ^{13}C NMR of Sm@C_{2v}(3)-C_{80} (125 MHz, CS_2, 293 K): δ =185.94(4C), 166.57(4C), 165.90(2C), 163.68(4C), 162.57(4C), 159.73(4C), 159.35(4C), 156.37(2C), 155.43(2C), 152.52(4C), 150.95(2C), 149.78(4C), 149.40(4C), 144.16(4C), 141.43(4C), 140.01(4C), 138.70(2C), 138.20(4C), 135.25(4C), 134.55(4C), 126.31(4C), 120.52(4C), and 115.60(2C) ppm.
29 *An Atlas of Fullerenes*, ed. P. W. Fowler and D. E. Manolopoulos, Clarendon Press, Oxford, 1995.
30 X. J. Xu, M. X. Li, Z. J. Shi and Z. N. Gu, *Chem.–Eur. J.*, 2006, **12**, 562.
31 T. Suzuki, K. Kikuchi, F. Oguri, Y. Nakao, S. Suzuki, Y. Achiba, K. Yamamoto, H. Funasaka and T. Takahashi, *Tetrahedron*, 1996, **52**, 4973.